Proceedings of the ASME 2011 International Mechanical Engineering Congress & Exposition
IMECE 2011
November 11-17, 2011, Denver, CO, USA

IMECE2011-64254

AN ISOTROPIC AUXETIC STRUCTURAL NETWORK WITH LIMITED SHEAR STIFFNESS

Alessandro Spadoni
Laboratory of Wave Mechanics of Multi-Field Interactions (LOMI)
Institute of Mechanical Engineering
École Polytechnique Fédérale de Lausanne
1015 Lausanne, Switzerland
Email: alex.spadoni@epfl.ch

ABSTRACT

The chiral lattice is a unique structural network not symmetric to its mirror image, and with a negative Poisson's ratio. Previous investigations have considered this structural network for the design of superior structural components with sandwich construction, but these were limited by the in-plane Poisson's ratio predicted to be exactly -1*. This paper presents estimates of the mechanical properties of the chiral lattice obtained from a multi-cell finite-element model. It is shown that the chiral lattice has a shear stiffness bound by that of the triangular lattice and it is very compliant to direct stresses. The minimum in-plane poisson's ratio is estimated to be* ≈ -0.94*.*

INTRODUCTION

Cellular solids possess superior mechanical properties [1] that can be exploited for the development of novel structured materials. Their wide-spread employment in the aerospace, automotive, and naval industries, among others, is to be attributed primarily to unique physical properties: low relative density, low electrical conductivity, low Young's modulus and strength [1]. Low density facilitates the design components with high specific (mass-normalized) stiffness, and provides effective thermal insulation [1, 2]. The latter is to be attributed to the low conductivity of the second phase, most often a gas. Low density is also ideal for naval applications where buoyancy and specific stiffness are required [1]. Low strength is very advantageous in applications where mechanical-energy absorption is paramount. This may be the case of crush-worthy materials, or of packaging materials for sensitive components, where foams are most applicable [1, 3]. The most recognizable application, however, is that of sandwich panels. This particular use of cellular structures exploits the high specific stiffness of the honeycomb core, as well as optimal distribution of inertia to produce components with extremely high bending stiffness [1, 3]. The introduction of affordable core materials and bonding techniques is responsible for widespread utilization of sandwich panels [3], which may feature both foam or honeycomb cores.

Cellular solids are both naturally-occurring and man-made materials or structures, depending on the characteristic length scale, and may feature both ordered (or deterministic) and disordered (or stochastic) topologies. Both stochastic and deterministic instances are characterized by assemblies of cells with solid boundaries, which may be beam-like and plate-like components yielding open and closed-cell configurations respectively [1]. Cellular solids possess a low relative density usually lower than 30% than that of their constituent material.

In addition to the constituent material, the effective mechanical properties of cellular solids are determined by the layout of slender internal members. Deterministic configurations in particular offer the possibility to design the effective mechanical behavior by appropriately choosing the structural arrangement of the microstructure. This particular capability was exploited to design a two-dimensional (2D), transversally isotropic, structural lattice with a negative Poisson's ratio, known as the chiral lattice [4]. The chiral lattice achieves a negative in-plane Pois-

son's ratio, also known as auxetic behavior [5], as a result of a deformation behavior strongly influenced by the presence of rotational units [4]. Auxetic behavior in isotropic media represents a rarity which is in fact to be attributed to two aspects of a material's microstructure: the presence of rotational units and non-affine deformation kinematics [6]. Both topology and mechanical behavior of the chiral lattice can be significantly altered via a single parameter known as the topology parameter [7].

The ability to set the elastic properties of a lattice, simply by changing a reduced set of geometric parameters, implies ease of mechanical tailoring to a given application. While traditionally different stiffness or compliance requirements have been addressed by employing purposely engineered structural arrangements, the possibility of exploring a large realm of elastic behavior by varying a single parameter may provide new possibilities, both for static and dynamic behavior. Previous studies reported in [4] suggest that the chiral lattice features a Poisson's ratio $\nu = -1$ indicating auxetic behavior, in addition to exhibiting isotropic mechanical characteristics. The Theory of Elasticity however restricts the Poisson's ratio of isotropic solids to $-1 < \nu < 1/2$ [8]. Any attempts to model an isotropic material with $\nu = -1$ by equivalent continuum models are thwarted by a resulting indeterminate constitutive matrix. The analyses presented in this manuscript are devoted to establishing the magnitude of the Poisson's ratio and of the Young's modulus more accurately with respect to the estimates presented in [4]. In particular,

In this manuscript, the elasto-static behavior of the chiral lattice is analyzed employing finite-element models. In particular, in-plane Young's modulus, shear modulus and Poisson's ratio are investigated and compared to the same constants of classical configurations like the square, triangular and hexagonal configurations.

OVERVIEW OF METHODS TO DETERMINE THE MECHANICS OF CELLULAR SOLIDS

Cellular solids feature low relative density and are commonly constituted by arrangements of beam-like slender components. For this reason, the elastic properties of cellular solids are ordinarily determined by employing beam theory to relate loads and corresponding deformations at the unit cell level, an example of which is shown in fig. 1. The simplest technique considers the symmetry of a specific unit cell and relates externally applied stresses to concentrated loads acting on the unit-cell members. The kinematics of the unit cell are then related to externally-applied stresses, yielding effective constants uniquely defining Hooke's Law for the equivalent material.

In the case of the hexagonal lattice depicted in fig. 1, non-affine deformations facilitate the determination of the mechanical behavior as only one topologically-distinct component of the unit cell elastically deflects. Externally applied loads are decomposed

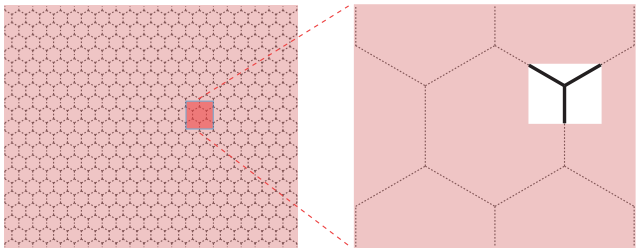

FIGURE 1. Microstructural detail (unit-cell members) in periodic solids [7].

into local stress components which can easily be associated to local deformations. Given the periodicity of the medium, the strain in a cell can be related to the global strain. With strains arising from applied tractions, effective material properties may be defined as a function of geometric parameters. Such analytical procedure leads to estimates of equivalent mechanical properties which are as accurate as the beam model employed to describe the deformation behavior [1]. The same technique has been applied to the square, hexagonal, triangular and Kagomé lattices among others [9]. More sophisticated beam theories may be employed to include shear effects in addition to axial, bending deformations.

A second method relates displacements at the extremities of the unit cell to those of a central joint, or node, relating them through a spatial Taylor-series expansion. This procedure is known as *Homogenization* and it is employed to describe the elasto-dynamic behavior of an equivalent continuum via two partial differential equations. The coefficients of such equations are compared to known equilibrium-equation forms such as Classical Elasticity Theory to obtain the equivalent Lamé constants. In a similar fashion, the method elucidated in [10], for elasto-static phenomena, relates Taylor-series-linearized displacements at the extremities of the unit cell to those of the central joint. The approximate kinematic variables are then employed to obtain an expression of the unit-cell strain energy in terms of geometric parameters of the lattice. The constitutive matrix relating stress components to strain components is obtained by taking derivatives of the approximated strain-energy function.

In a third procedure, the governing equations of motion, in stress formulation, are expressed in weak form and are solved numerically via the finite-element method. Internal forces acting on each of the beam-like members of the cellular solid are transformed into equivalent continuum stresses by averaging the same internal forces over a representative volume, usually at a scale (f ig. 1) comprising several unit cells [11, 12]. This particular technique allows the evaluation of global elasto-static phenomena bypassing the determination of elastic constants altogether. This analysis method is particularly suited for stochastic configu-

rations, for which it is not possible to determine elastic constants based on a unit-cell analysis, as the unit cell itself is only statistically described in terms of a characteristic volume or length scale. However, it is certainly applicable to deterministic configurations also, as demonstrated in [11, 12].

The unique topology of the chiral lattice investigated in this thesis, moreover, does not present a central joint, thus rendering Taylor-expansion-based techniques not easily applicable. Furthermore, one the objectives of this work is to classify the mechanical behavior of the chiral lattice in terms of its equivalent elastic constants, hence the stress-based formulation of [11,12] is not applicable either. In order to circumvent the difficulties posed by chiral topologies, an improved unit-cell analysis and macro-lattice models based on previous findings by [4] are employed with the objective of removing some of the limiting assumptions and approximations previously considered.

GEOMETRY OF THE CHIRAL LATTICE

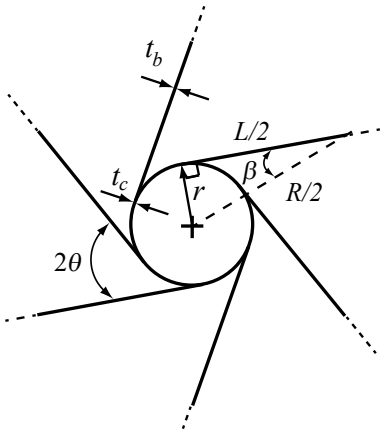

FIGURE 2. Geometry of the chiral lattice.

The chiral lattice shown in Fig. 2 consists of rings of radius r, acting as nodes, connected by ribs or ligaments, of length L tangent to the nodes themselves. The distance between node centers is denoted as R, while the angle between the imaginary line connecting the node centers and the ribs is defined as β. The angle between adjacent ligaments is denoted as 2θ. The wall thickness of nodes and ribs is denoted as t_c and t_b respectively.

Significantly different configurations can be obtained by varying the ratio L/R here denoted as the *topology parameter*. Possible topologies range from an hexagonal arrangement of rings ($L/R \to 0$) to the classic triangular lattice ($L/R \to 1$) as shown in Fig. 3. The ability to generate such topologically and mechanically different structural networks provides the unique opportunity of deriving a mechanical model that connects bending-dominated, axially-dominated, conventional, and auxetic lattices as a continuous function of the topology parameter. The same model could also bring a very interesting insight into the transition between bending-dominated behavior and axially dominated behavior which depend on ligament-wall thickness very differently. This implies that the relative density plays an important role in determining the mechanical response of the chiral assembly.

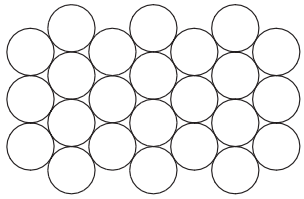

(a) $L/R \to 0$

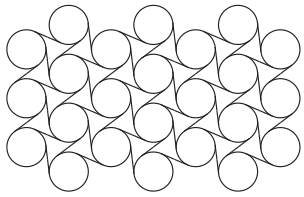

(b) $L/R = 0.60$

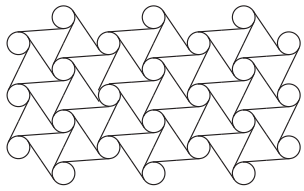

(c) $L/R = 0.90$

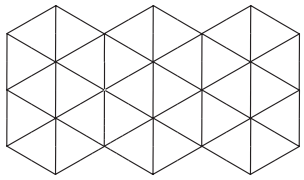

(d) $L/R \to 1$

FIGURE 3. Chiral-lattice geometry corresponding to increasing topology parameter L/R.

In the literature addressing auxetic materials, high specific shear modulus is often mentioned as one of the desirable features associated with auxetic behavior [4,5,13–15]. The findings

of [4] as discussed in the previous section however, do not allow the determination of such an elastic constant, because the Poisson's ratio is estimated to be exactly -1. Given the geometric hexagonal symmetry of the chiral lattice, it is legitimate to assume isotropic elasto-static characteristics. However as indicated by [8], the Poisson's ratio of isotropic materials is bounded by $-1 < \nu < 1/2$ in 3-D, or $-1 < \nu < 1$ in 2-D, and the associated constitutive matrix would become singular for $\nu = -1$.

MACRO-LATTICE FINITE-ELEMENT MODELS

In order to alleviate the shortcomings of the procedure above, the analysis proposed by [4] is revisited by relaxing the assumptions listed in the previous section. In the original investigations by [4], the following conditions were considered:

1.a nodes or circles are considered rigid;
1.b the kinematic behavior is imposed based on the experimental observations;
1.c internal forces oriented in a direction perpendicular to the externally applied stress are retained;
1.d axial and shear deformations of the ligaments are neglected;
1.e ligament wall thickness t_b is the same as that of the nodes or $t_b = t_c = t$;
1.f all deflections are small.

Some of the above assumptions are here relaxed, in order to obtain a refined estimate of the mechanical behavior of the chiral lattice. Ligament deformations here include bending as well as axial and shear deformations. The unusual kinematics of the chiral lattice featuring rotational units (the nodes) furthermore, prompts concerns with respect to neglecting any internal forces. Accordingly, resultant forces perpendicular to externally-applied stresses are here retained. The following conditions are considered:

2.a the deformations of nodes or circles are included in the analysis;
2.b no restrictions are placed upon resultant forces;
2 .c a macro-lattice FE model is employed;
2.d axial and shear deformations of the ligaments are included in the analysis;
2.e all deflections are small;
2.f ligament wall thickness t_b is the same as that of the nodes or $t_b = t_c = t$;

A FE model of the chiral lattice is employed to investigate the internal forces resulting from externally applied stresses, the extent of node deformations and the relation between equivalent elastic constants and geometric parameters. The commercially available FE software ANSYS® is employed. Specifically, Timoshenko beam elements featuring axial, bending and shear deflections are used. Each ligament is discretized by 24 elements, while each node or circle is discretized by 44 straight-beam elements. The base configuration is characterized by the parameters reported in Table. 1.

TABLE 1. Base configuration parameters of FE macro lattice

Geometric parameters	
L	1 m
L/R	$0.6 - 0.999$
t_b	0.01 m
t_c	0.01 m
b	0.01 m
Material properties: Aluminum	
E_s	71 GPa
ν_s	$1/3$

Given the structural composition of the chiral lattice, no single member is able to withstand a level of stress required to load the entire lattice. Perimeter circles on the sides perpendicular to the desired direction of deformation are kinematically constrained to be rigid, as depicted in fig. 4. A displacement producing the desired level of strain is applied at the center of each constrained perimeter circle. In order to avoid singularities in the stiffness matrix, a circle on each loaded side is constrained to displace collinearly with the loading direction. The analysis of shear stiffness, on the other hand, does not require any constraints perpendicularly to the imposed displacements of the perimeter nodes (fig. 4.c) as such boundary conditions ensure an invertible stiffness matrix. The effective applied stress is evaluated by summing the point forces at the center of each perimeter circle constrained kinematically and dividing by the loaded area, depicted as a yellow line in fig. 4. To estimate the shear stiffness the effective engineering strain is computed as follows:

$$\gamma_{yx} = \frac{v_{i+1} - v_i}{x_{i+1} - x_i} + \frac{u_{j+1} - u_j}{y_{j+1} - y_j}, \tag{1}$$

where (x, y) denote the location of the center of each node and (u, v) denote respectively displacements in the x and y directions. The subscripts i and j indicate node centers at the top and left sides of the lattice respectively. The equivalent elastic constants are then computed as: $E_x = \sigma_x/\varepsilon_x$ (fig. 4.a), $E_y = \sigma_y/\varepsilon_y$ (fig. 4.b), and $G_{yx} = \tau_{yx}/\gamma_{yx}$ (fig. 4.c). Poisson's ratios ν_{xy} and ν_{yx} are evaluated based on the displacements of the extremities of a unit cell

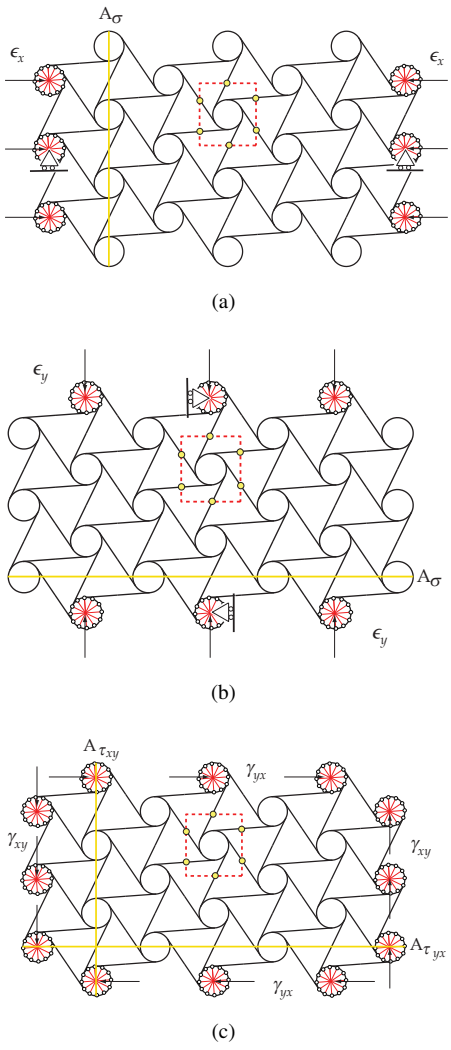

FIGURE 4. Representative FE macro-lattice configurations employed to study loading in the x-direction (a), y-direction (b) and xy-direction (c).

located approximately in the center of the lattice. The applicability of assumptions made with regard to internal forces, is investigated by monitoring the nodal-force values sampled at the extremities of a unit cell (yellow points in fig. 4), located approximately at the center of the lattice. For each of the three considered cases a strain level of 500 $\mu\varepsilon$ is employed.

A convergence study is carried out to establish the minimum number of cells necessary to reasonably estimate stress, strain, and associated elastic constants for each case considered, as well as to reduce the influence of boundary effects. Estimates of E_x shown in figs. 5 do not appear to approach an asymptotic value, suggesting that additional increments in cell numbers in the x and y-directions are required. Due to computing limitations, however, larger models are not feasible. A Richardson extrapolation [16] is used to obtain a limit value of Young's modulus to assess wether the current model size is appropriate. The limit

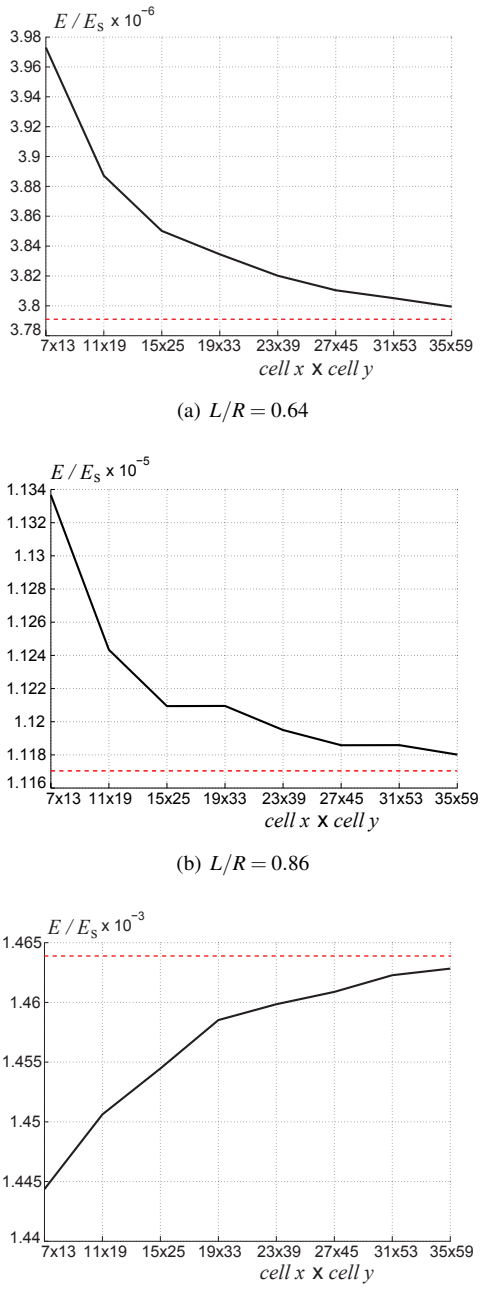

FIGURE 5. Variation of Young's modulus E_x with respect to lattice-cell number – – –, and extrapolated value – – – for three values of L/R

value of E_x, denoted as $\bar{E}_x$, may be expressed as:

$$\bar{E}_x = \lim_{c\to\infty} E_x(c), \tag{2}$$

where $E_x(c)$ is the FE approximation of $\bar{E}_x$ as a function of cell number c, and $c = cell\ x \times cell\ y$. The lattice cells considered here are those depicted in fig. 6. For $c \neq \infty$, eq. (2) may be expressed as:

$$\bar{E}_x - E_x(d) = a_n d^{k_n} + O\left(d^{k_{n+1}}\right),\ a_n \neq 0, \tag{3}$$

where n is an integer, a_n are unknown constants, k_n are known coefficients and $d = 1/c$. According to Richardson extrapolation [16], the term $a_n d^{k_n}$ in eq. (3) can be eliminated to obtain the following formula:

$$\bar{E}_x = \frac{r^{k_n} E_x(d/r) - E_x(d)}{r^{k_n} - 1} + O\left(d^{k_{n+1}}\right), \tag{4}$$

where $k_{n+1} > k_n$ and r is the refinement ratio or $r = d_{n+1}/d_n$. The value k_n represents the order of convergence, which is not known a priori. This may be found with the following expression [17] which considers three values of discretization:

$$k_n = ln\left(\frac{E_{x,3} - E_{x,2}}{E_{x,2} - E_{x,1}}\right)\frac{1}{ln(r)}. \tag{5}$$

For the Young's modulus estimates shown in fig. 5, $k_n \approx 2$. Neglecting the error of order $O\left(d^{k_{n+1}}\right)$ in eq. (4), the Young's modulus for an infinite lattice may be expressed as:

$$\bar{E}_x \cong \frac{r^{k_n} E_x(d/r) - E_x(d)}{r^{k_n} - 1}. \tag{6}$$

For the three sample values of topology parameter depicted in fig. 5, the difference between $E_x(d)$ computed with 35×59 cells and the extrapolated value $\bar{E}_x$ is within 0.3%. Given the small error introduced by limiting the FE lattice model to 35×59 cells of the kind depicted in fig. 6, and computational limitations, the maximum number of cells considered in fig. 5 is deemed legitimate as a basis for the estimation of the desired elastic constants.

RESULTS AND DISCUSSION

An estimate of Young's modulus based experimental observations is reported in [4] as $E_P = E_s\sqrt{3}\,(t/L)^3\,(L/r)^2$. This is compared to the Young's modulus obtained here E_U in fig. 7a for varying topology parameter L/R. The previous estimated of direct stiffness appear to overestimate the same measure obtained with FE models, especially for low values of L/R. This is to be expected as the original analysis in [4] neglected deformation of rings, which are very large for $L/R < 0.8$ (see fig. 3). For values of $L/R \to 1$, the two estimates of Young's modulus converge towards the upper bound represented by the direct stiffness of the triangular lattice E_T (fig. 3d). The chiral lattice is then significantly stiffer for configurations with small nodes or rings.

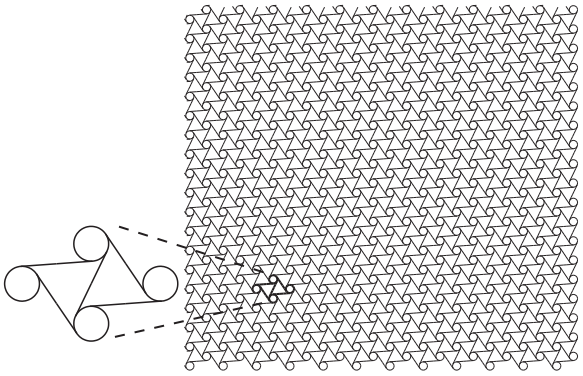

FIGURE 6. Chiral lattice employed for convergence studies

The computed Poisson's ratio is shown in fig. 7b, where both nu_{xy} and nu_{yx} are illustrated. The difference between the two is very small and on the order of numerical errors in the FE model. This suggested that the chiral lattice is indeed isotropic in plane as suggested in [4]. Moreover, Poisson's ratio is very sensitive to L/R and reaches a minimum of -0.94 for $L/R \approx 0.985$. This suggests that the chiral lattice indeed has a negative Poisson's ratio, but this depends on the particular configuration and approaches -1 but it is not exactly equal to this value. Following this minimum value, Poisson's ratio increases rapidly with a boundary-layer-like behavior to the limiting value of the triangular lattice for which $\nu = 1/3$ [10].

The FE models employed here indicate that the equivalent Poisson's ratio is not exactly -1. This removes the indeterminacy in the constitutive model of an equivalent medium with chiral-lattice microstructure. It is then possible to define a shear modulus, for which the estimated value from FE models is shown in fig. 7c. The shear stiffness, similarly to Young's modulus, is relatively low for configurations with large rings and increases rapidly to the limiting value of the triangular lattice G_T as $L/R \to 1$.

Comparison with Other Configurations

Auxetic materials like the chiral lattice are expected to have large shear stiffness [18–20], but given the findings summarized in fig. 7 it is apparent that is more compliant in shear than the triangular lattice (a non-auxetic configuration, that is $\nu \geq 0$). A comparison of the chiral lattice with other configurations is here suitable to shine light on some of the benefits, or lack therefor, offered by employing an auxetic microstructure to design materials with desired properties. In particular, square, triangular and hexagonal lattices are common topologies encountered in engineering applications and have been investigated for their superior specific (mass-normalized) properties [1, 9]. The equivalent mechanical properties for the aforementioned topologies in terms of geometric parameters are listed in Table. 2. where $\bar{\rho}$

TABLE 2. Mechanical properties of common lattice topologies (from [1, 9])

topology	$\bar{\rho}$	E/E_s	G/E_s	ν
square	$\frac{2t}{L}$	$\frac{1}{2}\bar{\rho}$	$\frac{1}{16}\bar{\rho}^3$	$\frac{1}{2}\nu_s\bar{\rho}$
triangular	$2\sqrt{3}\frac{t}{L}$	$\frac{1}{3}\bar{\rho}$	$\frac{1}{8}\bar{\rho}$	$1/3$
hexagonal	$\frac{2}{\sqrt{3}}\frac{t}{L}$	$\frac{3}{2}\bar{\rho}^3$	$\frac{3}{8}\bar{\rho}^3$	1.0

is the relative density, or the volume occupied by the internal members of a cellular solid normalized by the total volume occupied by a unit cell. For the chiral lattice, the relative density is $2\sqrt{3}\left(2\pi r t_c + 3L t_b\right)/\left(3R^2\right)$ [21]. The relative density varies with L/R as shown in fig. 8a. With relative density in hand, it is possible to compare mechanical properties of the chiral lattice with other configurations as summarized in Table 2. In particular, Young's moduli for the considered configurations are presented in fig. 8b, where the square and triangular lattices appear the stiffest. The chiral lattice is the most compliant of all, except for configurations with $L/R > 0.88$ in which case it is stiffer than the hexagonal lattice. The shear modulus however indicates excellent performance of the chiral lattice, only inferior that that of the triangular lattice (fig. 8c) for $L/R > 0.82$. In this case, the square and hexagonal lattices are more compliant.

The reason for the trends observed in figs. 8b and. 8c is the dependency of mechanical on relative density. Deformation mechanisms in 2-D lattices are determined by either bending or axial deformations of the internal members [22]. Mechanical properties associated with the former mechanism scale with $\bar{\rho}^3$, while those associated with the latter scale with $\bar{\rho}$ [22]. As the relative density for cellular solids is usually $\bar{\rho} \leq 30\%$ [1], $t/L \ll 1$. Mechanical properties associated with axial deformations are therefore much stiffer than those associated with bending. The Young's modulus for square and triangular configurations scales directly with the relative density as shown in Table 2 and it is thus higher than that of the hexagonal lattice which scales with $\bar{\rho}^3$ (fig. 8b). Chiral-lattice configurations are then dominated by bending deformations in response to direct stresses for $L/R < 0.98$, but this behavior changes to axial deformations for $L/R > 0.98$ (fig. 8b). On the other hand, the shear modulus of the triangular lattice is the highest since it scales with $\bar{\rho}$. The shear modulus of square and hexagonal honeycombs scales with $\bar{\rho}^3$ and it is accordingly low. Even though the chiral lattice presents a deformation mechanism dominated by bending deformations for $L/R < 0.98$, the computed shear modulus is higher than that for square and hexagonal honeycombs, but bounded by that of the triangular lattice.

CONCLUSIONS

This paper presents estimates of the mechanical properties of the chiral lattice obtained from a multi-cell finite-element model. This study is motivated by the indeterminacy in the mechanical model of an equivalent continuum with a chiral-lattice microstructure, since the Poisson's ratio determined in previous investigations is exactly -1. Refined estimates of the mechanical properties reported here show that the chiral lattice has a shear stiffness bound by that of the triangular lattice and it is very compliant to direct stresses. In particular, it is found that chiral-lattice configurations with large rings or nodes are dominated by bending deformations of the internal members in response to both direct stresses and shear. Accordingly, shear modulus and Young's modulus are lower than those for lattices dominated by axial deformations. Chiral lattice configurations with small rings or nodes have instead a much higher shear modulus than other bending-dominated lattices but are bound by the triangular lattice. Finally, the computed in-plane Poisson's ratio is estimated to be -0.94 for slender internal components. This removes the indeterminacy in establish a constitutive model for an equivalent continuum.

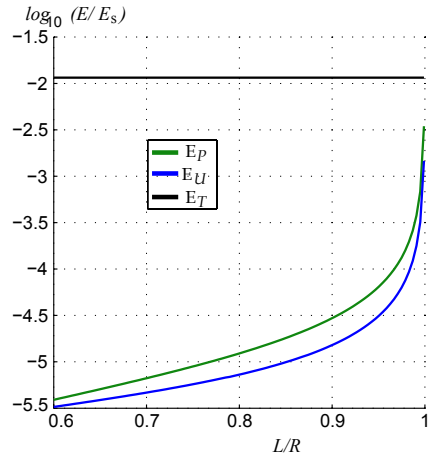

(a)

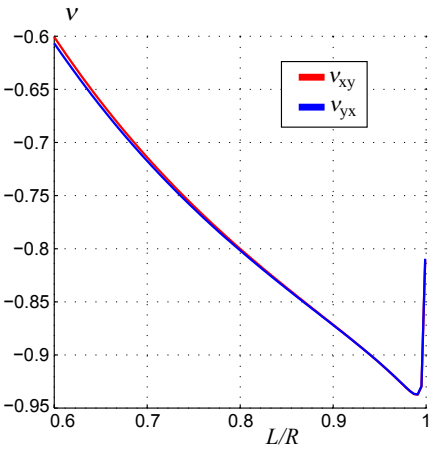

(b)

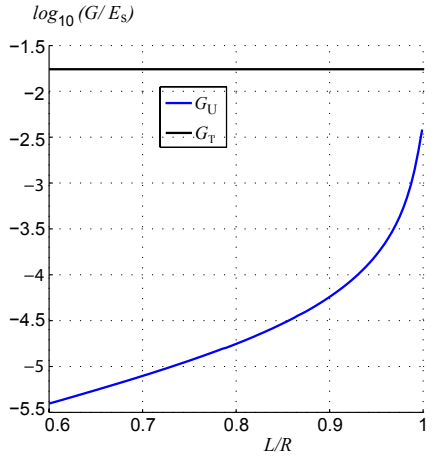

(c)

FIGURE 7. Young's modulus (a): E_U from FE models, previous estimate from [4] E_P, and that triangular lattice E_T. Computed Poisson's ratios ν_{xy} and ν_{yx} (b). comparison of shear modulus G_U with that of the triangular lattice G_T (c).

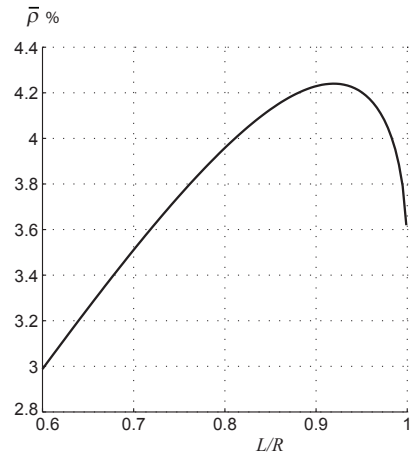

(a)

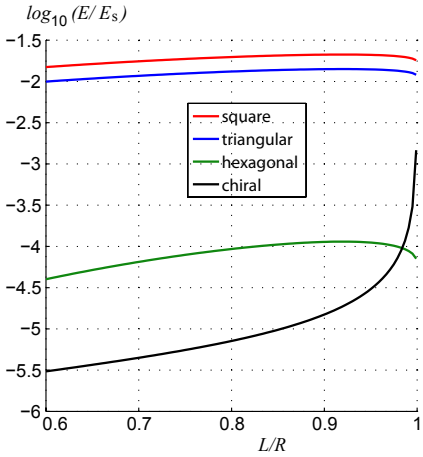

(b)

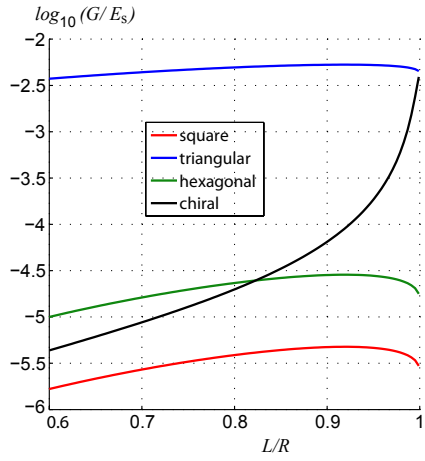

(c)

FIGURE 8. Relative density $\bar{\rho}$ (a) for the chiral lattice given $0.6 \leq L/R \leq 0.999$, $t = 0.01$ m and $L = 1$ m. Comparison of Young's modulus (b) and shear modulus (c) for various periodic topologies

REFERENCES

[1] Gibson, L. J., and Ashby, M. F., 1997. *Cellular solids: structure and properties*, second ed. Cambridge University Press.

[2] Hoff, N. J., 1955. "The thermal barrierstructures". *Trans. ASME*, pp. 759–763.

[3] Zenkert, D., ed., 1997. *The handbook of sandwich construction*. EMAS Publishing.

[4] Prall, D., and Lakes, R. S., 1996. "Properties of a chiral honeycomb with a poisson's ratio -1". *International Journal of Mechanical Sciences,* ***39***, pp. 305–314.

[5] Evans, K. E., Nkansah, M. A., Hutchinson, I. J., and Rogers, S. C., 1991. "Molecular network design". *Nature,* ***353***(6340), pp. 124–124.

[6] Lakes, R. S., 1991. "Deformation mechanisms in negative poisson's ratio materials: structural aspects". *Journal of Materials Science,* ***26***, pp. 2287–2292.

[7] Spadoni, A., 2008. "Application of chiral cellular materials for the design of innovative components". PhD thesis, Georgia Institute of Technology, August.

[8] Fung, Y., 1968. *Foundations of solid mechanics*. Prentice Hall.

[9] Wang, A. J., and McDowell, D. L., 2004. "In-plane stiffness and yield strength of periodic metal honeycombs". *Journal of engineering materials and technologies,* ***126***, pp. 137 – 156.

[10] Kumar, R., and McDowell, D., 2004. "Generalized continuum modeling of 2-D periodic cellular solids". *International Journal of Solids and Structures,* ***41***(26), pp. 7399–7422.

[11] Diebels, S., and Steeb, H., 2003. "Stress and couple stress in foams". *Computational Materials Science,* ***28***(3-4), pp. 714–722.

[12] Ebinger, T., Steeb, H., and Diebels, S., 2005. "Modeling macroscopic extended continua with the aid of numerical homogenization schemes". *Computational Materials Science,* ***32***(3-4), pp. 337–347.

[13] Grima, J. N., Gatt, R., and Farrugia, P.-S., 2008. "On the properties of auxetic meta-tetrachiral structures". *Physica Status Solidi B,* ***245***, pp. 511–520.

[14] Lakes, R. S., 1987. "Foam structures with a negative poisson's ratio". *Science,* ***235***, pp. 1038–1040.

[15] Sigmund, O., Torquato, S., and Aksay, I., 1998. "On the design of 1-3 piezocomposites using topology optimization". *Journal of Materials Research,* ***13***(4), pp. 1038 – 1048.

[16] Richardson, L. F., and Gaunt, J. A., 1927. "The deferred approach to the limit. part i. single lattice. part ii. interpenetrating lattices". *Philosophical Transactions of the Royal Society of London. Series A, containing papers of a mathematical or physical character,* ***226***, pp. 299–361.

[17] Roache, P. J., 1998. *Verification and validation in computational science and engineering*. Hermosa Publishers.

[18] Alderson, K., Pickles, A., Neale, P., and Evans, K., 1994. "Auxetic polyethylene: the effect of a negative poisson's ratio on hardness". *Acta Metall. Mater.,* ***42***(7), pp. 2261–2266.

[19] Evans, K. E., and Alderson, A., 2000. "Auxetic materials: Functional materials and structures from lateral thinking!". *Adv. Mater.,* ***12***(9), pp. 617–628.

[20] Lakes, R. S., and Elms, K., 1993. "Indentability of conventional and negative poisson's ratio foams". *J. Compos. Mater.,* ***27***(12), pp. 1193–1202.

[21] Spadoni, A., Ruzzene, M., Gonella, S., and Scarpa, F., 2009. "Phononic properties of hexagonal chiral lattices". *Wave Motion,* ***46***(7), pp. 435–450.

[22] Deshpande, V. S., Ashby, M. F., and Fleck, N. A., 2001. "Foam topology bending versus stretching dominated architectures". *Acta Mater.,* ***49***, pp. 1035–1040.